RANSAC for Aligned Planes with Application to Roof Plane Detection in Point Clouds

Steffen Goebbels and Regina Pohle-Fröhlich

Institute for Pattern Recognition, Faculty of Electrical Engineering and Computer Science,

Abstract: Random Sample Consensus (RANSAC) is a standard algorithm to recognize planes in point clouds. It does not require additional context information. However, it might be applied in situations where results can be improved based on domain knowledge. Such a situation is 3D building reconstruction from airborne laser scanning data. The normals of many roof facets are orthogonal to footprint vectors. This specific property helps to estimate roof planes more precisely. The paper describes the adapted RANSAC algorithm. It can be also used in other applications in which planes are aligned to supporting vectors.

1 INTRODUCTION

Semantic city models consist of building objects that are composed from walls, roof facets, windows, doors etc. Each wall and roof facet is defined by a planar polygon. Typically, such models are represented in CityGML, see (Gröger et al., 2012). One can reconstruct roofs from point clouds (often obtained by airborne laser scanning) using a model-driven, a data-driven or a hybrid approach that combines model- and data-driven methods, see (Tarsha-Kurdi et al., 2007b). In a model-driven approach, parameterized standard roofs from a catalogue are fitted to segments of the point cloud. This works well for standard roofs but not for scenic buildings like churches. Data driven methods detect single planes and combine them to a watertight roof (see e. g. (Elbrink and Vosselman, 2009; Kada and Wichmann, 2013)). To estimate such planes in point clouds, Random Sample Consensus (RANSAC) is a standard means, cf. (Yan et al., 2012), (Chen et al., 2014). It is regarded to lead to better results than the Hough transform (see (Tarsha-Kurdi et al., 2007a)). Our motivation is to improve roof plane detection with RANSAC in the context of data driven building reconstruction.

RANSAC was introduced as a much more general concept by Fischler and Bolles in (Fischler and Bolles, 1981). When applied to plane detection, the algorithm iteratively selects three (different) points. These points determine a plane if they are non-collinear. Then the algorithm counts inliers of this plane. An inlier is a point with a distance to the plane below a threshold value. In the original paper, the plane is chosen if the number of inliers exceeds another threshold value. Otherwise, the iteration is continued. To avoid this threshold parameter, in a common variant of RANSAC a predefined number of iterations is completed. Then a plane with a maximum count of inliers is chosen. The concept can be easily generalized to detect other geometric primitives (see the original paper (Fischler and Bolles, 1981) and, for example, (Schnabel et al., 2007) for some literature overview). In fact, RANSAC can be used to fit standard roofs in a model-driven approach, see (Henn et al., 2013) for a combination of RANSAC with machine learning. Due to our application of data-driven building model generation, we exclusively have to deal with planes. An important advantage is that RANSAC is robust against noise (cf. (Roth and Levine, 1993)) like, in our case, (sparse) vegetation, chimneys or antennas. A major disadvantage is computational cost. However, we do segment areas of possible roof planes prior to applying RANSAC. Such local point selection does speed-up the algorithm, see (Chen et al., 2014) and formula (3). Processing time becomes no issue.

RANSAC is independent of additional domain knowledge. It can be improved if additional information are given. For roof reconstruction, results can be enhanced by taking into account not only the number of inliers but also the variance of their distances to the candidate plane, see (Tarsha-Kurdi et al., 2008). A
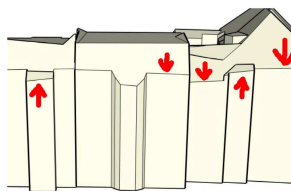
Figure 1: Roof planes were estimated with standard RANSAC on areas with homogeneous gradient directions of an airborne laser scanning point cloud: they are not perfectly aligned with footprint vectors.

more general approach is presented in (Saval-Calvo et al., 2015). Prior to RANSAC estimation, this method performs data clustering. Then planes are estimated iteratively on the clusters and evaluated by using domain specific constraints between clusters. Based on initial estimates, likely inter-plane relations (parallelism, orthogonality, etc.) can be established using optimization methods, e.g., see (Monszpart et al., 2015). In contrast to these additional alignment procedures, we directly consider simple, a-priori given domain knowledge within RANSAC. This knowledge is that most roof facets' normals should be orthogonal to a footprint edge. Footprint vectors are available in cadastral data. Also, many methods exist to extract footprints from point clouds or aerial images, cf. (Zeng et al., 2013). The main contribution of this paper is to utilize this knowledge to obtain estimated planes with normals that are properly aligned to footprint edges without the need of additional aligning procedures, see Figure 1. This is achieved in two steps, an extension to RANSAC that is described in the next section, and an optimization step that minimizes distances between inliers and plane with respect to keeping the alignment, see Section 3. We used these algorithms to compute a city model. Section 4 summarizes results.

2 ALGORITHM

2.1 Footprint Directions

Let $\vec{p} \in \mathbb{R}^2$ be a vector, then we denote its two components by $\vec{p}.x$ and $\vec{p}.y$. For vectors in $\mathbb{R}^3$ we denote the third component by $\vec{p}.z$. Let $G := \{\vec{g}_1, \ldots, \vec{g}_n\} \subset \mathbb{R}^2$ be a set of normalized footprint directions such that

$$\|\vec{g}_k\|_2 := \sqrt{\vec{g}_k.x^2 + \vec{g}_k.y^2} = 1.$$

We cluster footprint edges. Each cluster contains edges that point into the same or into the opposite direction or are orthogonal to these directions (see dark blue vectors in Figure 2). For each cluster, we sum

up the lengths of its edges. A most dominant direction is given by a cluster with a largest sum. For most buildings, it is sufficient that set G consists only of the most dominant direction. However, we also consider directions of all other clusters that have a sum above an application dependent threshold value of $2\,\text{m}$.
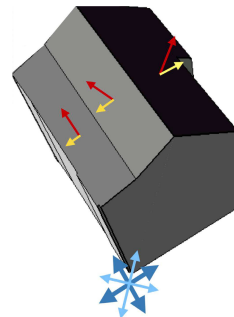

Figure 2: The footprint of the building leads to only one cluster of footprint directions. This cluster is defined by the four dark blue vectors. Red vectors are plane normals. Their projections onto a horizontal plane are drawn in yellow and have to be aligned to the dark blue footprint directions. The light blue vectors enclose 45° angles with the footprint directions and might also serve for alignment (cf. Section 4.)

2.2 Segmentation of Areas with Homogeneous Gradient Directions

If one directly uses RANSAC in connection with complex roof layouts, it is possible to detect spurious planes that do not match with roof facets. For example, such planes can be supported incidentally by points belonging to different parts of the roof such that these planes intersect with several real roof facets that provide inliers. To avoid such artifacts, one has to consider homogeneity of additional local features like gradients or normals, cf. (Schnabel et al., 2007), (Demir, 2018), (Poz and Ywata, 2019). RANSAC can be modified by using a soft threshold voting function based on this features, see (Xu et al., 2015). Another approach is to combine RANSAC with computation of Normal Distribution Transformation cells, see (Li et al., 2017). We follow the pre-segmentation approach described in (Goebbels and Pohle-Fröhlich, 2017) and the literature cited there. Solid structures in airborne laser scanning data basically are 2.5D. This can be utilized to represent a building's roof by a height-map image. The image can be generated based on a 2.5D triangulation of the sparse point cloud. On this height-map, flat and non-flat roof regions can be distinguished according to the lengths of gradients. Then non-flat roof regions can be further segmented according to homogeneous gradient directions, see Figure 3. To this end, one can determine the minima of a (smoothed) histogram of angles between

gradients and *x*-axis. Then angles between two consecutive minima define a cluster. Gradient directions with angles belonging to the same cluster are considered as homogeneous. We determine laser scanning points within connected components of such homogeneous height-map areas and apply RANSAC to this rather small filtered point clouds. Although height-map gradients approximately point into the same direction, the corresponding filtered point cloud might support multiple planes with different slopes (see left roof facets in Figure 2). It also may contain noise. Even a mean gradient direction might not be sufficiently precise to be used in plane detection because angle clusters are broad due to the interpolation technique that leads to height-maps. Thus one cannot directly fit a plane to a filtered point cloud by using regression approaches, segmentation does not make RANSAC unnecessary. However, apart from excluding spurious planes, filtering to smaller clouds does improve RANSAC performance very significantly.
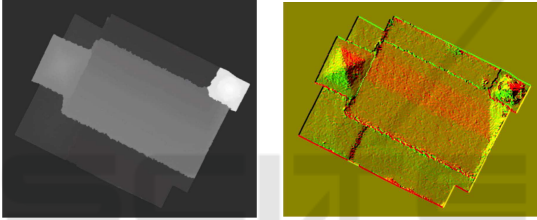

Figure 3: The left image is a height-map generated from laser scanning points by interpolation. Grey-values correspond to heights. Gradients on that height-map are visualized through colors in the right image by mapping their *x*- and *y*-coordinates to the red and green channels. Homogeneously colored areas are used to segment the point cloud such that RANSAC can be applied on segments.

For each connected component, we detect planes iteratively using the algorithm that is described in the next section. After identifying a plane, we remove its inliers from the corresponding filtered point cloud. Iterations terminate if numbers of inliers are below a threshold value.

2.3 RANSAC with Footprint Alignment

As standard RANSAC does, our variant also iteratively selects three points $\vec{p}_1$, $\vec{p}_2$, and $\vec{p}_3$. Within each iteration it computes a plane and counts the inliers if the selected points are non-collinear. In the end, a plane with the maximum number of inliers is selected. To avoid fragmented roofs, the (continued) selection of planes with largest inlier counts appears to be more suited than choosing planes with inlier counts above a threshold value. So far, there is no difference to standard RANSAC implementations. It

is also quite common (and already suggested in (Fischler and Bolles, 1981)) to improve the result by optimally fitting a plane through the best plane's inlier points. What makes our algorithm different is how the planes are determined if they are closely aligned to footprint edges.

Standard RANSAC directly computes a Hesse normal form that describes a plane through the selected three points. Using the outer product, one gets a normal

$$\vec{n}_0 := \frac{(\vec{p}_2 - \vec{p}_1) \times (\vec{p}_3 - \vec{p}_1)}{\|(\vec{p}_2 - \vec{p}_1) \times (\vec{p}_3 - \vec{p}_1)\|_2}$$

and a signed distance to the origin $\vec{0}$ that is given by the inner product

$$\rho_0 := <\vec{n}_0, \vec{p}_1> := \vec{n}_0.x \cdot \vec{p}_1.x + \vec{n}_0.y \cdot \vec{p}_1.y + \vec{n}_0.z \cdot \vec{p}_1.z.$$

A point $\vec{p}$ lies on this plane iff $<\vec{n}_0, \vec{p}> = \rho_0$.

We use normals that point upwards ("sign" denotes the signum function):

$$\vec{n}_1 := \text{sign}(\vec{n}_0.z) \cdot \vec{n}_0, \quad \rho_1 := \text{sign}(\vec{n}_0.z) \cdot \rho_0.$$

Therefore, $\vec{n}_1.z \geq 0$. If $\vec{n}_1.z \approx 0$ then the plane does not belong to a roof but to a wall. Thus, we can assume $\vec{n}_1.z > 0$. A flat roof is obtained iff $\vec{n}_1.z \approx 1$. In this case, we replace the normal by $(0,0,1)$ and adjust the distance ρ_1 to $\vec{0}$ by using the arithmetic mean of all inliers' z-coordinates (see Algorithms 1 and 3). In what follows we discuss the main case $0 < \vec{n}_1.z < 1$.

Most but not all roof facets might be aligned to footprint edges. We replace the normal $\vec{n}_1$ by an adjusted one that is orthogonal or parallel to a footprint direction iff the difference angle between both normals is small. To this end, let $\alpha > 0$ be a threshold angle near 0. We determine angles between footprint directions $\vec{g}_k \in G$ (as well as orthogonal vectors $(-\vec{g}_k.y, \vec{g}_k.x)$) and projections of the normal vectors to the *x*-*y*-plane by computing inner products. To this end, let $\vec{n}_2 := (\vec{n}_1.x, \vec{n}_1.y)/\|(\vec{n}_1.x, \vec{n}_1.y)\|_2$. For $k \in \{1, \ldots, n\}$ let

$$c_k := \vec{n}_2.x \cdot \vec{g}_k.x + \vec{n}_2.y \cdot \vec{g}_k.y,$$
$$d_k := \vec{n}_2.x \cdot (-\vec{g}_k.y) + \vec{n}_2.y \cdot \vec{g}_k.x.$$

- If $|c_{k_0}| = \max\{|c_k|, |d_k| : k \in \{1, \ldots, n\}\}$ and $|c_{k_0}| > \cos(\alpha)$ then we change the direction of the normal in the *x*-*y*-plane depending on the sign of c_{k_0}. Its new normalized direction is

$$\vec{h} := \text{sign}(c_{k_0}) \cdot \vec{g}_{k_0}.$$

- Otherwise, if $|d_{k_0}| = \max\{|c_k|, |d_k| : k \in \{1, \ldots, n\}\}$ and $|d_{k_0}| > \cos(\alpha)$, we change the direction according to

$$\vec{h} := \text{sign}(d_{k_0}) \cdot \vec{g}_{k_0}.$$

195

- Otherwise, no footprint vector can be used for alignment. However, some roofs have facets with normals that, if projected to the ground plane, enclose 45° angles with footprint edges. To also consider these directions, one could now replace directions $\vec{g}_k$ by $[\vec{g}_k + (-\vec{g}_k.y, \vec{g}_k.x)]/\sqrt{2}$, recompute c_k and d_k and re-perform previous two cases.

For the first two cases, we replace the normal $\vec{n}_1$ with

$$\vec{n} := (l \cdot \vec{h}.x, l \cdot \vec{h}.y, \sqrt{1 - l^2}) \qquad (1)$$

such that $\|\vec{n}\|_2 = 1$. Please note that the z-component can be chosen to be positive because $\vec{h}$ points approximately into the same direction as $\vec{n}_1$ within the x-y-plane. To specify parameter l, let indices $i \neq j \in \{1, 2, 3\}$ be chosen such that b, defined by

$$a := (\vec{p}_i.x - \vec{p}_j.x)\vec{h}.x + (\vec{p}_i.y - \vec{p}_j.y)\vec{h}.y,$$
$$b := \frac{|a|}{\sqrt{(\vec{p}_i.x - \vec{p}_j.x)^2 + (\vec{p}_i.y - \vec{p}_j.y)^2}},$$

becomes maximal. Due to non-collinearity of points and because walls are excluded, $b > 0$ and vectors $(\vec{p}_i.x - \vec{p}_j.x, \vec{p}_i.y - \vec{p}_j.y)$ and $\vec{h}$ are as close as possible to being parallel. Then parameter $0 \leq l < 1$ is determined such that the vector $\vec{p}_i - \vec{p}_j$ becomes orthogonal to $\vec{n}$. Thus, we require

$$0 = \langle (\vec{p}_i - \vec{p}_j), \vec{n} \rangle = l \cdot a + \sqrt{1 - l^2}(\vec{p}_i.z - \vec{p}_j.z)$$

such that $l^2 a^2 = (1 - l^2)(\vec{p}_i.z - \vec{p}_j.z)^2$ and

$$l = \frac{|\vec{p}_i.z - \vec{p}_j.z|}{\sqrt{a^2 + (\vec{p}_i.z - \vec{p}_j.z)^2}}$$

if $\vec{p}_i.z - \vec{p}_j.z \neq 0$ and $l := 0$ otherwise. The adjusted Hesse normal form then is given by normal $\vec{n}$, see (1), and signed distance $\rho := \langle \vec{p}_i, \vec{n} \rangle$ between $\vec{0}$ and the plane. Due to construction, the two points $\vec{p}_i$ and $\vec{p}_j$ lie on this aligned plane. Algorithm 1 summarizes the computation of plane parameters.

As in many RANSAC implementations, the plane with the largest number of inliers of all iterations is selected. Inliers of a plane with parameters $(\vec{n}, \rho)$ are points of the point cloud (segment) P with a shortest distance to the plane that is less then a threshold value δ, i.e., a point $\vec{p} \in P \subset \mathbb{R}^3$ is an inlier with respect to $\vec{n}$, ρ, and δ iff $| \langle \vec{p}, \vec{n} \rangle - \rho| < \delta$, see Algorithm 2. Let I be the corresponding set of inliers. Instead of just counting inliers, one could also consider the variance of distances between inliers and their plane to select a best plane, cf. (Tarsha-Kurdi et al., 2008). However, our post processing procedure in Section 3 already does minimize variance of distances between inliers and plane. Depending on available data, other

---

Algorithm 1: Estimation of a plane's Hesse normal form; the algorithm returns a pair of normal vector and signed distance between plane and origin.

procedure GETPLANEPARMS($\vec{p}_1, \vec{p}_2, \vec{p}_3, G$)
$\quad \vec{n}_0 := \frac{(\vec{p}_2 - \vec{p}_1) \times (\vec{p}_3 - \vec{p}_1)}{\|(\vec{p}_2 - \vec{p}_1) \times (\vec{p}_3 - \vec{p}_1)\|_2}$
$\quad \rho_0 := \langle \vec{n}_0, \vec{p}_1 \rangle$
$\quad$**if** $\vec{n}_0.z \approx 0$ **then return** $(\vec{n}_0, \rho_0)$ $\qquad \triangleright$ wall plane
$\quad \vec{n}_1 := \text{sign}(\vec{n}_0.z) \cdot \vec{n}_0$
$\quad \rho_1 := \text{sign}(\vec{n}_0.z) \cdot \rho_0$
$\quad$**if** $\vec{n}_1.z \approx 1$ **then return** $((0, 0, 1), \rho_1)$ $\qquad \triangleright$ flat roof
$\quad \vec{n}_2 := (\vec{n}_1.x, \vec{n}_1.y)/\|(\vec{n}_1.x, \vec{n}_1.y)\|_2.$
$\quad m := -1$
$\quad$**for** $\vec{g} \in G$ **do**
$\quad\quad c := \vec{n}_2.x \cdot \vec{g}.x + \vec{n}_2.y \cdot \vec{g}.y$
$\quad\quad$**if** $|c| > \cos(\alpha) \wedge |c| > m$ **then**
$\quad\quad\quad \vec{h} := \text{sign}(c) \cdot \vec{g}$
$\quad\quad\quad m := |c|$
$\quad\quad d := \vec{n}_2.x \cdot (-\vec{g}.y) + \vec{n}_2.y \cdot \vec{g}.x$
$\quad\quad$**if** $|d| > \cos(\alpha) \wedge |d| > m$ **then**
$\quad\quad\quad \vec{h} := \text{sign}(d) \cdot \vec{g}$
$\quad\quad\quad m := |d|$
$\quad$**if** $m = -1$ **then return** $(\vec{n}_1, \rho_1)$
$\qquad\qquad\qquad\qquad \triangleright$ normal can be adjusted
$\quad \vec{r}_1 := \vec{p}_1 - \vec{p}_2, \vec{r}_2 := \vec{p}_2 - \vec{p}_3, \vec{r}_3 := \vec{p}_1 - \vec{p}_3$
$\quad$**for** $i \in \{1, 2, 3\}$ **do**
$\quad\quad a_i := \vec{r}_i.x \cdot \vec{h}.x + \vec{r}_i.y \cdot \vec{h}.y$
$\quad\quad b_i := |a_i|/\sqrt{\vec{r}_i.x^2 + \vec{r}_i.y^2}$
$\quad$**for** $i \in \{1, 2, 3\}$ **do**
$\quad\quad$**if** $b_i = \max\{b_1, b_2, b_3\}$ **then**
$\quad\quad\quad a := a_i, \vec{r} := \vec{r}_i, \vec{p} := \vec{p}_i$
$\quad$**if** $\vec{r}.z = 0$ **then** l:=0;
$\quad$**else**
$\quad\quad l := \frac{|\vec{r}.z|}{\sqrt{a^2 + \vec{r}.z^2}}$
$\quad \vec{n} := (l \cdot \vec{h}.x, l \cdot \vec{h}.y, \sqrt{1 - l^2})$
$\quad$**return** $(\vec{n}, \langle \vec{p}, \vec{n} \rangle)$

---

strategies for defining inliers might be helpful. In case of a colored point cloud, one could additionally match color information, see (Adam et al., 2018). Instead of searching for inliers in the original point cloud, we also tested with points obtained from the 2.5D height-map, equidistantly arranged in the x-y-plane. We expected that, due to interpolation, some artificial step edges between roof facets could be avoided. But only in rare cases a different plane was selected as best fitting.

It is well known (see (Fischler and Bolles, 1981)) that standard RANSAC at least needs

$$i \geq \ln(1 - p)/\ln\left(1 - \left(\frac{|I|}{|P|}\right)^3\right) \qquad (2)$$

iterations to find three inlier points of a specific plane with a probability of at least p. For this specific plane, $|I|/|P|$ is the probability to randomly select one inlier, where $|I|$ is the number of all inliers of this plane and

$|P|$ is the size of the point cloud. Thus $1 - (|I|/|P|)^3$ is the probability to independently draw three points from P such that at least one is no inlier. The chance that this happens in each of i independent experiments is $(1 - (|I|/|P|)^3)^i$. This probability has to be less than $1 - p$ which gives (2). The exponent 3 equals the number of points needed to define the geometric primitive. The formula does not consider that collinear inliers could be selected. To reduce the probability of getting collinear points, it is better to draw three points without repetition, i.e., to draw three different points. Then points are no longer drawn independently. Instead of multiplying probabilities to get p^3, the probability

$$\frac{\binom{|I|}{3}}{\binom{|P|}{3}} = \frac{|I|}{|P|} \cdot \frac{|I|-1}{|P|-1} \cdot \frac{|I|-2}{|P|-2}$$

now is given by the hypergeometric distribution, i.e.,

$$i \geq \ln(1-p) / \ln\left(1 - \frac{|I|}{|P|} \cdot \frac{|I|-1}{|P|-1} \cdot \frac{|I|-2}{|P|-2}\right). \quad (3)$$

In order to use formulas (2) or (3) as a lower bound for the number of RANSAC iterations, one has to conservatively estimate inlier ratio $\mu := \frac{|I|}{|P|}$ and replace unknown $|I|$ by $\mu \cdot |P|$.

But even three pairwise different points could lie on a straight line. Since the two-dimensional volume of any finite union of straight lines is zero, the probability of randomly scanning a point that precisely lies on at least one line through any two previously scanned points is zero. However, laser scanners do not place points randomly but in stripes. Then the probability of finding three collinear inliers depends on unknown geometric properties. For example, if we assume a regular $\sqrt{|P|} \times \sqrt{|P|}$ grid for x-y-coordinates (that occurs if one applies RANSAC on a 2.5D height-map) then at most $\sqrt{|P|}$ inliers can lie on a line. We assume $\sqrt{|P|} < |I|$. Then with

$$\ln(1-p) / \ln\left(1 - \frac{|I|}{|P|} \cdot \frac{|I|-1}{|P|-1} \cdot \frac{|I|-\sqrt{|P|}}{|P|-2}\right)$$

iterations, the probability to get three non-collinear inliers is above p.

Even if three non-collinear points are drawn, they lie within threshold distance but probably not exactly on the specific plane we are looking for. A plane that is supported by the three points might have an inlier count that differs from the count of the specific plane. This are all reasons to consider additional iterations.

Algorithm 2: RANSAC for roof plane detection in point cloud P using footprint directions in set G. Number of iterations is i, threshold value $\delta > 0$ is used to define inliers.

procedure GETINLIERS($\vec{n}$, ρ, P, δ)
   $I := \emptyset$
   for $\vec{p} \in P$ **do**
      if $|<\vec{p},\vec{n}> -\rho| < \delta$ **then**
         $I := I \cup \{\vec{p}\}$
   return I
procedure RANSAC(P, G, i, δ)
   $I_{best} := \emptyset, k = 1$
   while $(k \leq i) \wedge (|I_{best}| < |P|)$ **do**
      randomly select different points $\vec{p}_1, \vec{p}_2, \vec{p}_3 \in P$
      if $\det[\vec{p}_1, \vec{p}_2, \vec{p}_3] \neq 0$ **then** ▷ non-collinear points
         $(\vec{n}, \rho) :=$ GETPLANEPARMS($\vec{p}_1, \vec{p}_2, \vec{p}_3, G$)
         if $\vec{n}.z \not\approx 0$ **then** ▷ no wall
            $I :=$ GETINLIERS($\vec{n}$, ρ, P, δ)
            if $|I| > |I_{best}|$ **then**
               $I_{best} := I, \vec{n}_{best} := \vec{n}, \rho_{best} := \rho$
      $k := k + 1$
   if $|I_{best}| > 2$ **then return** $(\vec{n}_{best}, \rho_{best}, I_{best})$
   else
      return "no plane found"

3 OPTIMIZING PLANES' SLOPES

RANSAC provides a plane with a maximum number of inliers. However, there might exist a different plane with the same set of inliers but smaller distances between inliers and plane. While keeping alignment to footprint vectors, we find such a "better" plane by applying a principal component analysis (PCA), see Figure 4. For building model reconstruction, most estimated planes are indeed aligned to footprint directions (see Section 4). Thus, we have to find an optimal value for a parameter l such that shortest distances between inliers and plane become minimal with a nor-
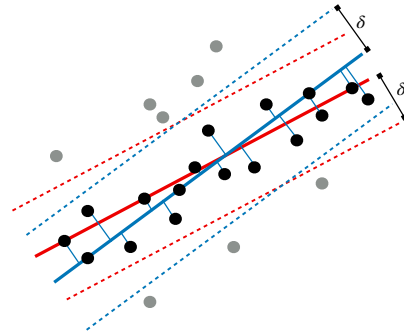

Figure 4: The bold red and blue lines visualize cuts through planes that are already aligned to a footprint vector. Both planes have the same inliers (black dots) with respect to a threshold value δ. But the sum of squared distances (squared lengths of thin blue lines in case of the blue plane) is not minimal for both planes. A best fitting plane should be computed.

mal vector

$$\vec{n}_{\mathrm{opt}} := \left(l \cdot \vec{d}.x, l \cdot \vec{d}.y, \sqrt{1 - l^2} \right) \qquad (4)$$

where $\vec{d} = \frac{(\vec{n}.x, \vec{n}.y)}{\|(\vec{n}.x, \vec{n}.y)\|_2}$. This means that we maintain the direction of the normal vector with respect to its x- and y-coordinates. If aligned to a footprint direction, a plane keeps aligned. To find l, we orthogonally project all inliers to the plane spanned by vectors $(\vec{d}.x, \vec{d}.y, 0)$ and $(0,0,1)$. The origin $\vec{0}$ lies on this plane. For numerical stability it might be required to shift the plane by adding an inlier such that numbers become smaller. We add inlier $\vec{q}_1$ which is element of the set $I := \{\vec{q}_1, \ldots \vec{q}_m\} \subset \mathbb{R}^3$ of all inliers. We obtain the 2D set of projections $\{\vec{t}_1, \ldots \vec{t}_m\} \subset \mathbb{R}^2$ via

$$
\begin{aligned}
\vec{t}_k.x &:= \ < (\vec{q}_k - \vec{q}_1), (\vec{d}.x, \vec{d}.y, 0) >, \\
\vec{t}_k.y &:= \ < (\vec{q}_k - \vec{q}_1), (0,0,1) > = \vec{q}_k.z - \vec{q}_1.z.
\end{aligned}
$$

For this set, we perform a PCA to find the best fitting line. To obtain the covariance matrix

$$C = \left[\begin{array}{cc} \sigma_x^2 & \sigma_{xy} \\ \sigma_{xy} & \sigma_y^2 \end{array} \right],$$

let $\bar{\vec{t}} := \frac{1}{m} \sum_{k=1}^m \vec{t}_k$ be the center of gravity of the 2D points,

$$\sigma_x^2 := \frac{\sum_{k=0}^m (\vec{t}.x - \bar{\vec{t}}.x)^2}{m-1}, \ \sigma_y^2 := \frac{\sum_{k=0}^m (\vec{t}.y - \bar{\vec{t}}.y)^2}{m-1},$$

$$\sigma_{xy} := \frac{1}{m-1} \sum_{k=0}^m (\vec{t}.x - \bar{\vec{t}}.x)(\vec{t}.y - \bar{\vec{t}}.y).$$

A largest eigenvalue of C or $(m-1)C$ is

$$\lambda = \frac{\sigma_{xx} + \sigma_{yy}}{2} + \sqrt{\frac{(\sigma_{xx} + \sigma_{yy})^2}{4} - (\sigma_{xx} \sigma_{yy} - \sigma_{xy}^2)},$$

a corresponding eigenvector $\vec{e}$ is given via $(-\sigma_{xy}, \sigma_x^2 - \lambda)$ or $(\sigma_y^2 - \lambda, -\sigma_{xy})$ if non-zero. Parameter l of $\vec{n}_{\mathrm{opt}}$ in (4) has to be chosen such that $(l, \sqrt{1-l^2})$ becomes orthogonal to $\vec{e}$, i.e.,

$$l \cdot \vec{e}.x + \sqrt{1-l^2} \cdot \vec{e}.y = 0$$

such that $l^2 \cdot (\vec{e}.x)^2 = (1-l^2) \cdot (\vec{e}.y)^2$. The positive solution is $l = |\vec{e}.y| / \|\vec{e}\|_2$. With the optimized normal $\vec{n}_{\mathrm{opt}}$, the signed distance between plane and $\vec{0}$ has to be updated as well. To this end, we use the center of gravity of projected points:

$$\rho_{\mathrm{opt}} := \ < (\vec{q}_1.x + \bar{\vec{t}}.x \cdot \vec{d}.x, \vec{q}_1.y + \bar{\vec{t}}.x \cdot \vec{d}.y, \bar{\vec{t}}.y), \vec{n}_{\mathrm{opt}} > .$$

The optimization procedure is summarized in Algorithm 3.

After all roof planes of a building are determined, the data-driven approach of roof reconstruction can be combined with model knowledge. Typically, a building only has very few different roof slopes. By clustering z-components of normals, similar z-values can be adjusted to a mean value. Also, similar facade heights can be balanced by adjusting distances of planes to the origin.

Algorithm 3: Optimization of plane parameters.

procedure OPTIMIZEPLANE($\vec{n}$, ρ, I)
  $d = \frac{(\vec{n}.x, \vec{n}.y)}{\|(\vec{n}.x, \vec{n}.y)\|_2}$
  $T := \emptyset$ ▷ T is a multiset or list.
  $\bar{\vec{t}} := \vec{0} \in \mathbb{R}^2$
  select an inlier $\vec{q}_1 \in I$.
  for $\vec{q} \in I$ **do**
    $\vec{t}.x := \ < (\vec{q} - \vec{q}_1), (\vec{d}.x, \vec{d}.y, 0) >$
    $\vec{t}.y := \vec{q}.z - \vec{q}_1.z.$
    $T := T \cup \{\vec{t}\}, \bar{\vec{t}} := \bar{\vec{t}} + \vec{t},$
  $\bar{\vec{t}} := \bar{\vec{t}} / |I|,$
  if $\vec{n}.z = 1$ **then return** $(\vec{n}, \bar{\vec{t}}.y)$
  else
    $s_x^2 := s_y^2 := s_{xy} := 0$
    for $\vec{t} \in T$ **do**
      $s_x^2 := s_x^2 + (\vec{t}.x - \bar{\vec{t}}.x)^2, s_y^2 := s_y^2 + (\vec{t}.y - \bar{\vec{t}}.y)^2$
      $s_{xy} := s_{xy} + (\vec{t}.x - \bar{\vec{t}}.x)(\vec{t}.y - \bar{\vec{t}}.y)$
    $\lambda := \frac{s_{xx} + s_{yy}}{2} + \sqrt{\frac{(s_{xx} + s_{yy})^2}{4} - (s_{xx} s_{yy} - s_{xy}^2)}$
    $\vec{e}_1 := (-s_{xy}, s_x^2 - \lambda), \vec{e}_2 := (s_y^2 - \lambda, -s_{xy})$
    if $\|\vec{e}_1\|_2 > \|\vec{e}_2\|_2$ **then** $\vec{e} := \vec{e}_1$
    else
      if $\|\vec{e}_2\|_2 > 0$ **then** $\vec{e} := \vec{e}_2$
      else $\vec{e} := (1,0)$
    $l := \frac{|\vec{e}.y|}{\|\vec{e}\|_2}$
    $\vec{n}_{\mathrm{opt}} := \left(l \cdot \vec{d}.x, l \cdot \vec{d}.y, \sqrt{1 - l^2} \right)$
  $\rho_{\mathrm{opt}} := \ < (\vec{q}_1.x + \bar{\vec{t}}.x \cdot \vec{d}.x, \vec{q}_1.y + \bar{\vec{t}}.x \cdot \vec{d}.y, \bar{\vec{t}}.y), \vec{n}_{\mathrm{opt}} >$
  return $(\vec{n}_{\mathrm{opt}}, \rho_{\mathrm{opt}})$

---

4 RESULTS

We tested with data of one square kilometer. It belongs to the city of Dortmund and covers zone 32U UTM-interval $[393000, 394000] \times [5703000, 5704000]$, see Figure 5. This area consists of 1,591 buildings or building parts. We chose $\alpha = 5°$ as a threshold angle for aligning with footprint directions and $\delta = 0.1\,\mathrm{m}$ as threshold distance to define inliers. This value is compliant with precision of airborne laser scanning. Due to pre-segmentation and analysis of our data, we conservatively expected more than $\mu = 30\%$ of points to be inliers of the largest plane to be detected with each call of RANSAC. For large point clouds P we can approximate (3) with (2). If we want to find three inliers of the largest plane with a probability of 99.999% then we should consider more than 420 iterations. For conservative results, we used 500 RANSAC iterations in which three pairwise different (but not necessarily non-collinear) points were selected. With these parameters and because of pre-segmentation, detected planes had a mean inlier ratio of 89.5%, see Figure 6. The 0.25-quantile is 81.9% such that only 15 iterations would

Figure 5: Test data: Our variant of RANSAC was used to estimate roof facets of this model of a square kilometer of the city of Dortmund.
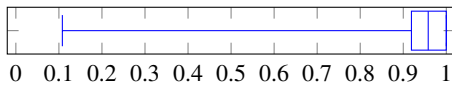

Figure 6: Boxplot of best planes' inlier ratios.

have been sufficient to detect 75% of model planes.

When considering only footprint directions with a minimum length of 2 m, 7,616 facet normals of non-flat roofs were at least slightly aligned. The remaining 2,845 facets of non-flat roofs pointed into different directions.

The mean change of x-y-projections of best fitting planes' normals was 1.5°. The diagrams in Figure 7 show the distribution of smallest angles between footprint edges and projected original, non-adjusted normals of best fitting planes.
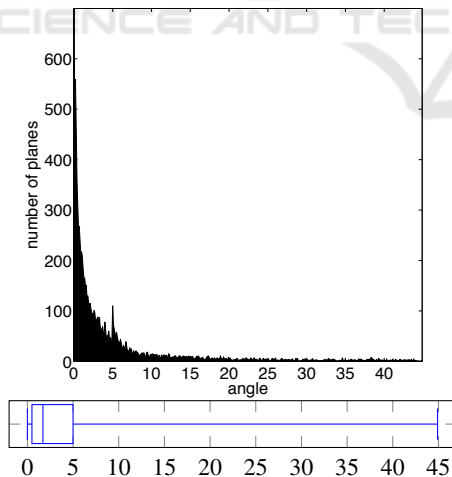

Figure 7: Minimum angles between estimated plane normals (projected to the x-y-plane) and footprint directions.

The effect of PCA normalization for non-flat roofs is shown in Figure 8. The average change of normal angles is 1.67°. Indeed, the optimization step does contribute to the quality of estimated planes.
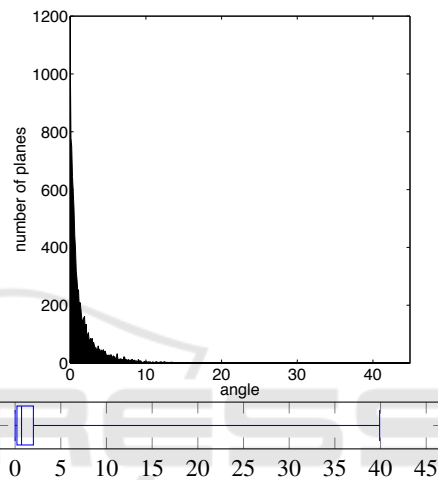

Figure 8: Angle changes due to PCA optimization.

If one also allows alignment to lines that enclose 45° angles with footprint vectors then 7,926 out of 10,461 non-flat roof facets were aligned.

5 CONCLUSIONS

The described method is limited to planar roof facets. Although changes of models are not immediately visible, more precise roof geometries can be obtained by aligning normal vectors to footprint directions. This makes it easier to maintain planarity of roof facets when combining them without introducing artificial step edges. In some cases, aligned roof facets also reduce the number of roof polygons. Alignment can be used to speed-up RANSAC. In our application, most but not all the planes can be aligned to a footprint vector. However in case of alignment, the footprint vector could be selected due to our pre-segmentation according to gradient angles. If such additional information is available for all planes to be detected, one can use two instead of three (non-collinear) points to define a

plane. Then only

$$\frac{\ln(1-p)}{\ln\left(1 - \frac{|I|}{|P|} \cdot \frac{|I|-1}{|P|-1}\right)} < \frac{\ln(1-p)}{\ln\left(1 - \frac{|I|}{|P|} \cdot \frac{|I|-1}{|P|-1} \cdot \frac{|I|-2}{|P|-2}\right)}$$

iterations are required to find different inliers of the plane with probability p, see (3). Future work could incorporate texture information from oblique areal images.

ACKNOWLEDGEMENTS

We thank Cornelia Herrmann-Hahn from Dortmund cadastral office for inspiring this work.

REFERENCES

Adam, A., Chatzilari, E., Nikolopoulos, S., and Kompatsiaris, I. (2018). H-RANSAC: A hybrid point cloud segmentation combining 2D and 3D data. *ISPRS Ann. Photogramm. Remote Sens. and Spatial Inf. Sci.*, IV-2:1–8.

Chen, D., Zhang, L., Mathioupoulos, P. T., and Huang, X. (2014). A methodology for automated segmentation and reconstruction of urban 3-D buildings from ALS point clouds. *IEEE Journal of Selected Topics in Applied Earth Observations and Remote Sensing*, 7(10):4199–4217.

Demir, N. (2018). Automated detection of 3D roof planes from lidar data. *Journal of the Indian Society of Remote Sensing*, 46(8):1265–1272.

Elbrink, S. O. and Vosselman, G. (2009). Building reconstruction by target based graph matching on incomplete laser data: analysis and limitations. *Sensors*, 9(8):6101–6118.

Fischler, M. A. and Bolles, R. C. (1981). Random sample consensus: a paradigm for model fitting with applications to image analysis and automated cartography. *Communications of the ACM*, 24(6):381–395.

Goebbels, S. and Pohle-Fröhlich, R. (2017). Quality enhancement techniques for building models derived from sparse point clouds. In *Proc. International Conference on Computer Graphics Theory and Applications (GRAPP) 2017*, pages 93–104, Porto.

Gröger, G., Kolbe, T. H., Nagel, C., and Häfele, K. H. (2012). *OpenGIS City Geography Markup Language (CityGML) Encoding Standard. Version 2.0.0*. Open Geospatial Consortium.

Henn, A., Gröger, G., Stroh, V., and Plümer, L. (2013). Model driven reconstruction of roofs from sparse lidar point clouds. *ISPRS Journal of Photogrammetry and Remote Sensing*, 76:17–29.

Kada, M. and Wichmann, A. (2013). Feature-driven 3D building modeling using planar halfspaces. *ISPRS Ann. Photogramm. Remote Sens. and Spatial Inf. Sci.*, II-3/W3:37–42.

Li, L., Yang, F., Zhu, H., Li, D., Li, Y., and Tang, L. (2017). An improved RANSAC for 3D point cloud plane segmentation based on Normal Distribution Transformation cells. *Remote Sensing*, 9(433):1–16.

Monszpart, A., Mellado, N., Brostow, G., and Mitra, N. (2015). Rapter: Rebuilding man-made scenes with regular arrangements of planes. *ACM Transactions on Graphics*, 34:103:1–103:12.

Poz, A. P. D. and Ywata, M. S. Y. (2019). Adaptive random sample consensus approach for segmentation of building roof in airborne laser scanning point cloud. *International Journal of Remote Sensing*, online first:1–15.

Roth, G. and Levine, M. D. (1993). Extracting geometric primitives. *CVGIP: Image Underst.*, 58(1):1–22.

Saval-Calvo, M., Azorin-Lopez, J., Fuster-Guillo, A., and Garcia-Rodriguez, J. (2015). Three-dimensional planar model estimation using multi-constraint knowledge based on k-means and RANSAC. *Applied Soft Computing*, 34:572–586.

Schnabel, R., Wahl, R., and Klein, R. (2007). RANSAC based out-of-core point-cloud shape detection for city-modeling. *Schriftenreihe des DVW, Terrestrisches Laser-Scanning (TLS 2007)*.

Tarsha-Kurdi, F., Landes, T., and Grussenmeyer, P. (2007a). Hough-transform and extended RANSAC algorithms for automatic detection of 3D building roof planes from lidar data. *ISPRS International Archives of Photogrammetry, Remote Sensing and Spatial Information Systems*, XXXVI(W52):407–412.

Tarsha-Kurdi, F., Landes, T., and Grussenmeyer, P. (2008). Extended RANSAC algorithm for automatic detection of building roof planes from LIDAR data. *The Photogrammetric Journal of Finland*, 21(7):97–109.

Tarsha-Kurdi, F., Landes, T., Grussenmeyer, P., and Koehl, M. (2007b). Model-driven and data-driven approaches using LIDAR data: Analysis and comparison. *International Archives of Photogrammetry, Remote Sensing and Spatial Information Sciences*, 36(3/W49A):87–92.

Xu, B., Jiang, W., Shan, J., Zhang, J., and Li, L. (2015). Investigation on the weighted RANSAC approaches for building roof plane segmentation from lidar point clouds. *Remote Sensing*, 8(5):1–23.

Yan, J., Jiang, W., and Shan, J. (2012). Quality analysis on RANSAC-based roof facets extraction from airborne LIDAR data. *International Archives of Photogrammetry and Remote Sensing*, XXXIX(B3):367–372.

Zeng, C., Wang, J., and Lehrbass, B. (2013). An evaluation system for building footprint extraction from remotely sensed data. *IEEE Journal of Selected Topics in Applied Earth Observations and Remote Sensing*, 6(3):1640–1652.